JACS
JOURNAL OF THE AMERICAN CHEMICAL SOCIETY
Communication
pubs.acs.org/JACS

Facile Conversion of Hydroxy Double Salts to Metal–Organic Frameworks Using Metal Oxide Particles and Atomic Layer Deposition Thin-Film Templates

Junjie Zhao,[†] William T. Nunn,[†] Paul C. Lemaire,[†] Yiliang Lin,[†] Michael D. Dickey,[†] Christopher J. Oldham,[†] Howard J. Walls,[‡] Gregory W. Peterson,[#] Mark D. Losego,[§] and Gregory N. Parsons*[,†]

[†]Department of Chemical and Biomolecular Engineering, North Carolina State University, Raleigh, North Carolina 27695, United States

[‡]RTI International, Research Triangle Park, North Carolina 27709, United States

[#]Edgewood Chemical Biological Center, Aberdeen Proving Ground, Maryland 21010, United States

[§]School of Materials Science and Engineering, Georgia Institute of Technology, Atlanta, Georgia 30332, United States

Supporting Information

ABSTRACT: Rapid room-temperature synthesis of metal–organic frameworks (MOFs) is highly desired for industrial implementation and commercialization. Here we find that a (Zn,Cu) hydroxy double salt (HDS) intermediate formed *in situ* from ZnO particles or thin films enables rapid growth (<1 min) of HKUST-1 ($Cu_3(BTC)_2$) at room temperature. The space-time-yield reaches $>3 \times 10^4$ kg·m^{-3}·d^{-1}, at least 1 order of magnitude greater than any prior report. The high anion exchange rate of (Zn,Cu) hydroxy nitrate HDS drives the ultrafast MOF formation. Similarly, we obtained Cu-BDC, ZIF-8, and IRMOF-3 structures from HDSs, demonstrating synthetic generality. Using ZnO thin films deposited via atomic layer deposition, MOF patterns are obtained on pre-patterned surfaces, and dense HKUST-1 coatings are grown onto various form factors, including polymer spheres, silicon wafers, and fibers. Breakthrough tests show that the MOF-functionalized fibers have high adsorption capacity for toxic gases. This rapid synthesis route is also promising for new MOF-based composite materials and applications.

Metal–organic frameworks (MOFs) are a class of crystalline porous materials that exhibit high surface area and large pore volume.[1] Versatile combinations of MOF constituents enable structural design and pore size control,[2] and post-synthetic modification can introduce additional internal functionality.[3] While MOFs are promising for gas adsorption and separation,[4] catalysis/photocatalysis,[5] chemical sensing,[6] and other applications,[7] the low synthesis rates (space-time-yield (STY) typically <300 kg·m^{-3}·d^{-1}) and harsh processing conditions (high temperature and pressure) of traditional solvothermal methods still remain as major hurdles for industrial implementation of MOFs and MOF-functionalized composites.[8] New synthetic routes are highly desired to enable fast MOF formation at room temperature (rt).

Several strategies have been attempted to tackle this challenge, including mechanochemical methods,[9] irradiation-assisted synthesis,[10] and electrochemical approaches.[11] While these methods can reduce the reaction time and synthesis temperature for MOF production, large amounts of external energy input are required to enable the chemical reactions. Recently, metal oxides and hydroxides have been reported to act as nucleating agents or sources of cations for rt MOF synthesis.[12,13] However, the incorporation of residual oxide/hydroxide seeds within the MOF crystals due to insufficient conversion affects the purity and properties of these MOFs. Although extending the reaction time to >1 h[12] or increasing the reaction temperature to ≥95 °C[13] can reduce the oxide/hydroxide residue in the final product, alternative approaches with rapid conversion at ∼25 °C are still needed.

Here we report a novel synthesis method using hydroxy double salts (HDSs) as intermediates. HDSs are layered compounds consisting of cationic sheets connected by inorganic/organic interlamellar anions.[14] These materials are generally synthesized by reacting one divalent metal oxide with another different divalent cation. Similar to layered double hydroxides, HDSs show excellent anion exchangeability and are promising for catalysis[15] and pharmaceutical applications.[16] We discovered that HDSs can undergo facile conversion and enable rapid formation of MOFs at rt. Our STY for HKUST-1 ($Cu_3(BTC)_2$) reaches 3.6×10^4 kg·m^{-3}·d^{-1}, at least 1 order of magnitude greater than any prior report.[8,11,12]

Figure 1a depicts our rapid rt approach for synthesizing HKUST-1 powder. $Cu(NO_3)_2$ aqueous solution and DMF are added to ZnO nanoslurries (dispersed in H_2O, average particle size 252 ± 23 nm, Figure S1) at rt to form a light blue suspension of (Zn,Cu) hydroxy nitrate HDS. H_3BTC ethanolic solution is immediately added to the suspension, turning it to a turquoise color in ∼10 s (Video S1)—a definitive visual indication of HKUST-1 formation. The powder product was immediately

Received: August 24, 2015
Published: October 11, 2015

DOI: 10.1021/jacs.5b08752
J. Am. Chem. Soc. 2015, 137, 13756–13759

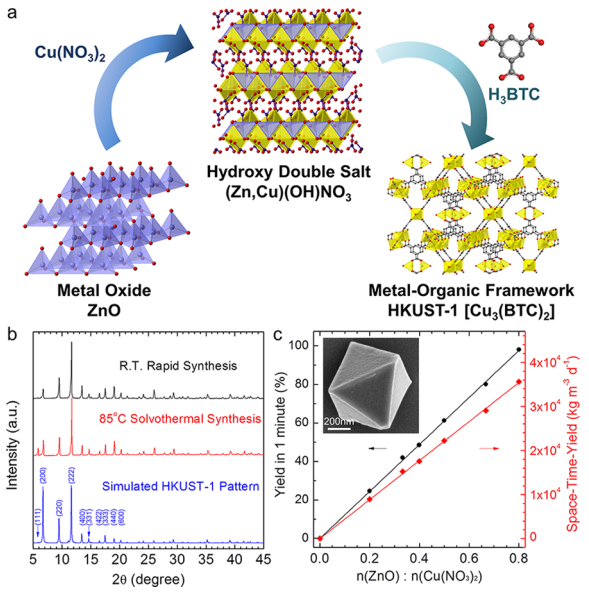

Figure 1. (a) Schematic of the rapid room-temperature synthesis of HKUST-1. ZnO reacts with $Cu(NO_3)_2$ to form (Zn,Cu) HDS, which converts to HKUST-1 via fast anion exchange. (b) Powder XRD patterns for HKUST-1 synthesized in rapid rt method (black) and solvothermal method (red), and simulated HKUST-1 pattern (blue). (c) Percent yield in 1 min of reaction (black circle) and space-time-yield for the rapid rt synthesis (red diamond). Inset: SEM image of a HKUST-1 crystal showing the octahedral shape.

filtered and washed with ethanol after 1 min of reaction, and subsequently dried in a vacuum oven at 120 °C for 6 h.

Figure 1b compares simulated and experimental X-ray diffraction (XRD) patterns for HKUST-1 powders obtained from rapid rt synthesis and 85 °C solvothermal synthesis. All peak positions match the simulated pattern, indicating the product synthesized from HDS is crystalline HKUST-1. The MOF powder synthesized at 85 °C shows a somewhat larger (111) peak, possibly a result of dehydration and rehydration. The sharp XRD peaks confirm good crystallinity of the HKUST-1.

Scanning electron microscopy (SEM) images (inset in Figure 1c and Figure S2a,b) show the MOF particles obtained from the rapid synthesis have an average size of 1.17 ± 0.40 μm (Figure S2c). The octahedron crystal shape is also consistent with previous observations for this fcc-type MOF crystal.[17] After the rapid MOF synthesis, ZnO residue was not observed by SEM or XRD, and no Zn was detected on the MOF surface by energy-dispersive X-ray (EDX) analysis (Figure S3) or time-of-flight secondary ion mass spectroscopy (ToF-SIMS) (Figure S4). Inductively coupled plasma optical emission spectroscopy (ICP-OES) was also used to characterize the concentration of Zn^{2+} residue in the HKUST-1 powder after degrading the crystals in strong acids and H_2O_2.[18] ICP-OES data (Table S1) show the Zn^{2+} concentration is generally <0.70 wt%, demonstrating high purity within the HKUST-1 crystals.

We evaluated the BET surface area of the HKUST-1 powder based on the N_2 adsorption isotherm measured at 77 K. Figure S5 shows the N_2 adsorption and desorption curves for the powder prepared via rapid synthesis. The average BET surface area (1895 ± 84 m^2/g) is high compared to previous reports,[17,19] also suggesting the high purity of the MOF, as any residue with low surface area will precipitously reduce the MOF BET surface area.

Figure 1c shows STY ($kg \cdot m^{-3} \cdot d^{-1}$) for the rapid rt synthesis and the yield after 1 min of reaction. Both the STY and the yield increase linearly as a function of the $n(ZnO):n(Cu(NO_3)_2)$ molar ratio ($n(H_3BTC):n(Cu(NO_3)_2)$ was kept at 1:1.8). Previous high-throughput synthesis methods for HKUST-1 show STY ranging from 225 to 1842 $kg \cdot m^{-3} \cdot d^{-1}$.[11,12] Our synthesis strategy reaches an STY up to 3.6×10^4 $kg \cdot m^{-3} \cdot d^{-1}$, an improvement of >1 order of magnitude. The yield also reaches up to 98% in just 1 min of reaction, showing significant promise for scale-up processing. While a further increase of the $n(ZnO):n(Cu(NO_3)_2)$ ratio can lead to a higher apparent yield, a corresponding drop in the BET surface area indicates incomplete HDS conversion due to insufficient H_3BTC reactant. By maintaining the ratio $n(ZnO):n(Cu(NO_3)_2) \leq 0.8$, all HKUST-1 samples show BET surface area exceeding 1800 m^2/g.

We hypothesized that HDS could be the critical intermediate during the rapid rt MOF synthesis, because (Zn,Cu) hydroxy nitrate HDS can be converted from ZnO and has been reported with a high reaction rate for anion exchange.[14] To understand the reaction mechanism for the rapid MOF growth, we investigated particularly how HDS forms and how it converts to MOF. Specifically, ZnO thin films (34.4 ± 0.6 nm) were deposited on IR-transparent silicon wafers via atomic layer deposition (ALD) and soaked in $Cu(NO_3)_2$ aqueous solution for 1 min, followed by XRD analysis. The resulting XRD pattern (Figure 2a) matches well with prior reports for (Zn,Cu) hydroxy nitrate.[14] Subsequently, the HDS was exposed to H_3BTC solution ($DMF:H_2O:EtOH$ = 1:1:1 volume ratio) for only 30 s, and analyzed by XRD. The XRD peaks representative for HKUST-1 in the corresponding pattern and octahedron crystals found on the surface in SEM images (Figure S6) confirm the formation of the targeted MOF. The decreased intensity of HDS XRD peaks indicates HDS is partially consumed after the short exposure to H_3BTC.

Figure 2b shows FTIR difference spectra collected for ALD ZnO thin film in the as-deposited form and after sequential

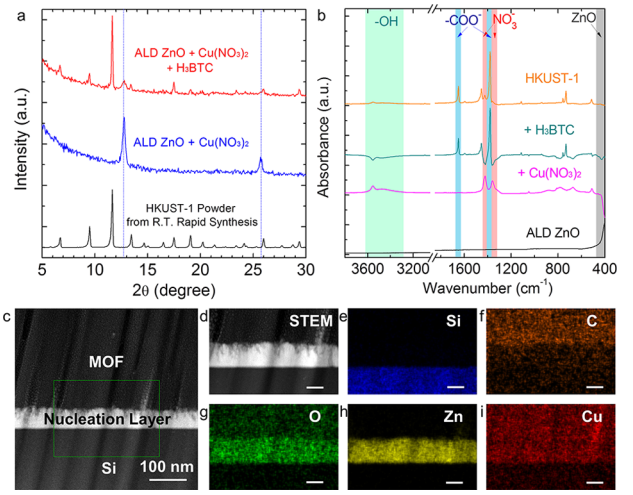

Figure 2. (a) XRD patterns for HKUST-1 powder (black), ALD ZnO surface after 1 min exposure to $Cu(NO_3)_2$ (blue) and then to H_3BTC for 30 s (red). Blue dotted lines represent the (Zn,Cu) HDS. (b) FTIR difference spectra for ALD ZnO as-deposited (black, Si as background), after 1 min exposure to $Cu(NO_3)_2$ (magenta, previous spectrum as background), and after 30 s exposure to H_3BTC (green, previous spectrum as background), and the final HKUST-1 spectrum (orange, Si as background). (c,d) HAADF-STEM images for a cross section of the HKUST-1 grown on ALD ZnO-coated Si wafer. The green box in (c) indicates the location of (d–i). (e–i) High-resolution EDX mapping images of the cross section. Scale bars = 50 nm.

DOI: 10.1021/jacs.5b08752
J. Am. Chem. Soc. 2015, 137, 13756–13759

Table 1. Routes for HDS-Driven Room-Temperature Synthesis of Various MOF Materials from ZnO

metal salt	HDS	organic linker	MOF	HDS-to-MOF time (min)
$Cu(NO_3)_2$	(Zn,Cu)	H_3BTC	HKUST-1	1
$Cu(NO_3)_2$	(Zn,Cu)	H_2BDC	Cu-BDC	2
$Zn(OAc)_2$	(Zn,Zn)	2-MeIm	ZIF-8	10
$Zn(OAc)_2$	(Zn,Zn)	H_2BDC-NH_2	IRMOF-3	10

exposure to $Cu(NO_3)_2$ and H_3BTC solutions. After the film soaked in $Cu(NO_3)_2$ aqueous solution for 1 min, the negative-going mode between 400 and 480 cm^{-1} confirms loss of ZnO, and the appearance of $\nu(NO_3^-)$ (1360 and 1420 cm^{-1}) and the distinct O−H group modes (~3300−3620 cm^{-1}) indicates the formation of hydroxy nitrate.[20] After subsequent exposure to the H_3BTC solution for 30 s, the peaks for NO_3^- and O−H diminish, while the symmetric (1378 cm^{-1}) and asymmetric (1649 cm^{-1}) stretching modes for the carboxylate groups appear. This spectrum change clearly reveals the anion exchange process in the (Zn,Cu) HDS, and further supports our proposed reaction path (Figure 1a): ZnO reacts with $Cu(NO_3)_2$ to form (Zn,Cu) HDS, followed by rapid anion exchange between NO_3^- and OH^- in the HDS and BTC^{3-}, yielding ultrafast formation of HKUST-1 at rt.

We further studied reactions on the ZnO surface when it was exposed simultaneously to both $Cu(NO_3)_2$ and H_3BTC. ALD ZnO (58.0 ± 0.6 nm) on a Si wafer was soaked in the mixed precursor solution for 5 min without stirring. Cross sections of the resulting thin films were imaged using high-angle annular dark-field scanning transmission electron microscopy (HAADF-STEM, Figure 2c,d), and the elemental distribution in the cross section was analyzed by high-resolution EDX mapping (Figure 2e−i). Figure 2c shows the abrupt interface between the nucleation layer and the Si substrate, and Figure 2h indicates Zn is present only in the nucleation layer. The nucleation layer also shows a uniformly distributed Cu signal in addition to Zn and O, further evidence for the formation of (Zn,Cu) HDS. The C, O, and Cu signals in the MOF layer are consistent with HKUST-1. These results indicate that the HDS is an important intermediate even in a one-pot batch procedure.

To demonstrate the generality of HDS for MOF synthesis, we synthesized three other MOFs via HDS intermediates. Table 1 summarizes these reaction routes (XRD in Figures S7−S9). We formed (Zn,Zn) hydroxy acetate HDS by reacting ZnO with $Zn(CH_3CO_2)_2{\cdot}2H_2O$ in deionized water at rt for 24 h.[21] ZIF-8 and IRMOF-3 were obtained from this (Zn,Zn) HDS within 10 min at rt. Furthermore, (Zn,Cu) HDS converts quickly (within 2 min) to Cu-BDC MOF. In addition to ZnO, CuO and NiO can also react with Zn^{2+}, Cu^{2+}, Ni^{2+}, and Co^{2+} salts to form HDS,[14] but most reported methods to synthesize these HDSs are slow (several days) and may require elevated temperature. Thus, these HDS are not desirable intermediates for rapid rt MOF synthesis. Important factors for analogous schemes will also include the solubility of organic linkers and the mobility of linkers in HDS lattices.

The rapid rt synthesis method is not limited to forming bulk MOF powder but also applicable for MOF patterns and thin-film coatings. Figure 3a briefly describes the fabrication procedure for patterning HKUST-1. We prepared SU-8 (negative photoresist) patterns on the ALD ZnO surface using photolithography and then exposed the patterned ZnO surface to $Cu(NO_3)_2$ and H_3BTC solutions sequentially. SEM and EDX images (Figure 3b−e) of a star-shape pattern reveal the selective HKUST-1 growth on ZnO surface. More optical micrographs of the MOF patterns are shown in Figure S10.

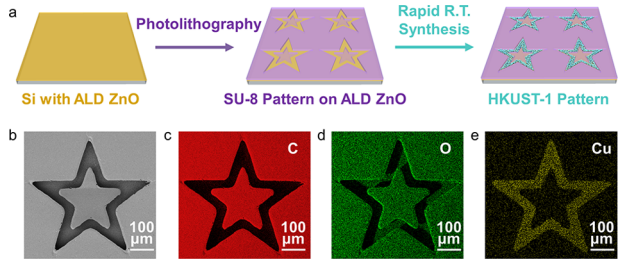

Figure 3. (a) Schematic of the fabrication of HKUST-1 patterns. (b−e) SEM image and EDX mapping for star-shape HKUST-1 pattern.

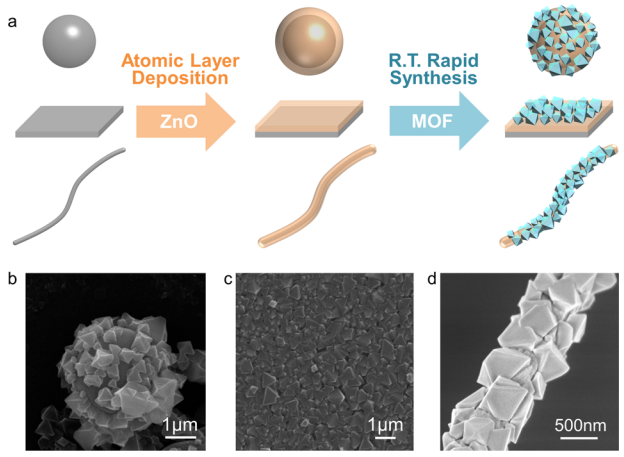

Figure 4. (a) Schematic of the rapid room-temperature synthesis of MOF coatings on various form factors. (b−d) SEM images of HKUST-1 deposited onto PS spheres, Si wafer, and PAN nanofibers, respectively.

Figure 4a illustrates the general approach to grow HKUST-1 thin films onto various form factors. Taking advantage of ALD,[22] we can deposit conformal ZnO thin films with controlled thickness on substrate materials with varied morphologies, such as polystyrene (PS) spheres, Si wafers, and polyacrylonitrile (PAN) fibers. Within 1 min of exposure to the HKUST-1 mother solution, dense coatings of HKUST-1 are also obtained on the above-mentioned ZnO-coated substrates (Figure 4b−d). Note that the substrate morphology is maintained with the conformal ALD ZnO thin films (200 cycles, ~36 nm). The coatings of densely packed crystals shown in Figure 4b−d therefore solely represent the HKUST-1 MOF. More SEM and TEM images for MOF-coated PS spheres, polypropylene (PP) microfibers, and PAN nanofibers are shown in Figures S11 and S12.

Previously, we showed that ALD Al_2O_3 promotes HKUST-1 solvothermal synthesis and layer-by-layer growth.[23] Here, using HDS formed from ALD ZnO thin films, we reduced the synthesis time to the scale of minutes. This is also the first example showing fast fabrication of MOF-functionalized fibrous materials at rt. By avoiding long exposure to heated organic solvents, we expect this synthesis route will enable more MOF-based composite structures, especially for delicate substrate materials that degrade at high temperature.

To demonstrate the functionality of these MOF-integrated materials, we characterized and compared the adsorption capacity of MOF-coated PP microfibers (MOF-PP) and PAN nanofibers (MOF-PAN). BET analysis based on N_2 isotherm (Figure 5a) shows the overall surface area is 201 and 524 m^2/

DOI: 10.1021/jacs.5b08752
J. Am. Chem. Soc. 2015, 137, 13756−13759

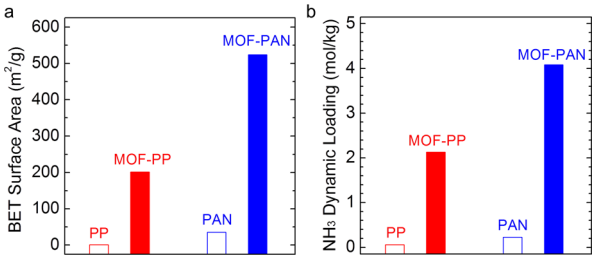

Figure 5. (a) BET surface area and (b) NH_3 dynamic loading for untreated PP microfibers and PAN nanofibers, and MOF-coated PP and PAN fibers (MOF-PP, MOF-PAN, respectively).

$g_{MOF+Fiber}$ for MOF-PP and MOF-PAN, respectively. The larger external surface area on nanofibers enables higher MOF mass loading, leading to a larger overall BET surface area.

Breakthrough tests were also performed to quantify the performance for hazardous gas removal. Figure 5b compares the NH_3 dynamic loadings on PP and PAN fiber mats with and without MOF coatings. Untreated PP and PAN fibers can barely retain the NH_3 challenge gas, while MOF-PP and MOF-PAN exhibit 36× and 18× higher dynamic loadings toward ammonia than the corresponding untreated fibers. In addition to NH_3, our MOF-functionalized fibers also show high adsorption capacity for H_2S (Figure S14), another highly toxic industrial chemical. These results all suggest the fibrous materials with MOF coatings are promising for gas filtration and protective garments.

In summary, we have discovered an ultrafast room-temperature MOF synthesis strategy using hydroxy double salt intermediates. (Zn,Cu) hydroxy nitrate HDS formed *in situ* from ZnO shows a high rate of anion exchange in the linker solution and drives the rapid formation of HKUST-1. The space-time-yield for HKUST-1 reaches 3.6×10^4 $kg \cdot m^{-3} \cdot d^{-1}$, >1 order of magnitude higher than previous published reports.[11,12] A similar synthetic strategy has been applied to Cu-BDC, ZIF-8, and IRMOF-3, demonstrating the synthetic generality. Using ALD ZnO thin films, we have successfully obtained HKUST-1 patterns and dense MOF coatings on PS microspheres, Si wafers, and PP and PAN fiber mats at a fast processing rate at room temperature. The HDS-driven MOF synthesis approach reported here is expected to dramatically improve MOF production rates and widely expand the material set of MOF-functionalized composites.

■ ASSOCIATED CONTENT

Supporting Information

The Supporting Information is available free of charge on the ACS Publications website at DOI: 10.1021/jacs.5b08752.

Experimental details, Tables S1 and S2, and Figures S1–S14 (PDF)

Video S1, showing synthesis of HKUST-1 MOF (ZIP)

■ AUTHOR INFORMATION

Corresponding Author

*gnp@ncsu.edu

Notes

The authors declare no competing financial interest.

■ ACKNOWLEDGMENTS

The authors acknowledge funding from ECBC (grant no. W911SR-07-C-0075) and the Joint Science and Technology Office (Army Research Office grant no. W911NF-13-1-0173). M.D.L. acknowledges Georgia Tech startup funds. The authors also acknowledge the use of the Analytical Instrumentation Facility at North Carolina State University, supported by the State of North Carolina and the National Science Foundation. We thank Roberto Garcia for TEM sample preparation, Yang Liu for HAADF-STEM, Chuanzhen Zhou for ToF-SIMS, Kim Hutchison for ICP-OES, and Matthew Browe for breakthrough tests.

■ REFERENCES

(1) Furukawa, H.; Cordova, K. E.; O'Keeffe, M.; Yaghi, O. M. *Science* **2013**, *341*, 1230444.

(2) Eddaoudi, M.; Kim, J.; Rosi, N.; Vodak, D.; Wachter, J.; O'Keeffe, M.; Yaghi, O. M. *Science* **2002**, *295*, 469.

(3) Sadakiyo, M.; Yamada, T.; Kitagawa, H. *J. Am. Chem. Soc.* **2014**, *136*, 13166. Brozek, C. K.; Dincă, M. *Chem. Soc. Rev.* **2014**, *43*, 5456.

(4) Britt, D.; Tranchemontagne, D.; Yaghi, O. M. *Proc. Natl. Acad. Sci. U. S. A.* **2008**, *105*, 11623. Li, J.-R.; Kuppler, R. J.; Zhou, H.-C. *Chem. Soc. Rev.* **2009**, *38*, 1477. Li, K.; Olson, D. H.; Seidel, J.; Emge, T. J.; Gong, H.; Zeng, H.; Li, J. *J. Am. Chem. Soc.* **2009**, *131*, 10368.

(5) Lee, J.; Farha, O. K.; Roberts, J.; Scheidt, K. A.; Nguyen, S. T.; Hupp, J. T. *Chem. Soc. Rev.* **2009**, *38*, 1450. Wang, C.; Xie, Z.; deKrafft, K. E.; Lin, W. *J. Am. Chem. Soc.* **2011**, *133*, 13445.

(6) Kreno, L. E.; Leong, K.; Farha, O. K.; Allendorf, M.; Van Duyne, R. P.; Hupp, J. T. *Chem. Rev.* **2012**, *112*, 1105.

(7) Meek, S. T.; Greathouse, J. A.; Allendorf, M. D. *Adv. Mater.* **2011**, *23*, 249. Horcajada, P.; Gref, R.; Baati, T.; Allan, P. K.; Maurin, G.; Couvreur, P.; Ferey, G.; Morris, R. E.; Serre, C. *Chem. Rev.* **2012**, *112*, 1232.

(8) Stock, N.; Biswas, S. *Chem. Rev.* **2012**, *112*, 933.

(9) Beldon, P. J.; Fábián, L.; Stein, R. S.; Thirumurugan, A.; Cheetham, A. K.; Friščić, T. *Angew. Chem., Int. Ed.* **2010**, *49*, 9640. Klimakow, M.; Klobes, P.; Thünemann, A. F.; Rademann, K.; Emmerling, F. *Chem. Mater.* **2010**, *22*, 5216.

(10) Khan, N. A.; Jhung, S. H. *Bull. Korean Chem. Soc.* **2009**, *30*, 2921. Zou, F.; Yu, R.; Li, R.; Li, W. *ChemPhysChem* **2013**, *14*, 2825.

(11) Müller, U.; Pütter, H.; Hesse, M.; Wessel, H.; Schubert, M.; Huff, J.; Guzmann, M. International Patent WO/2005/049892, 2005. Müller, U.; Schubert, M.; Teich, F.; Pütter, H.; Schierle-Arndt, K.; Pastré, J. *J. Mater. Chem.* **2006**, *16*, 626.

(12) Majano, G.; Pérez-Ramírez, J. *Adv. Mater.* **2013**, *25*, 1052.

(13) Zanchetta, E.; Malfatti, L.; Ricco, R.; Styles, M. J.; Lisi, F.; Coghlan, C. J.; Doonan, C. J.; Hill, A. J.; Brusatin, G.; Falcaro, P. *Chem. Mater.* **2015**, *27*, 690.

(14) Meyn, M.; Beneke, K.; Lagaly, G. *Inorg. Chem.* **1993**, *32*, 1209.

(15) Hara, T.; Ishikawa, M.; Sawada, J.; Ichikuni, N.; Shimazu, S. *Green Chem.* **2009**, *11*, 2034.

(16) Bull, R. M. R.; Markland, C.; Williams, G. R.; O'Hare, D. *J. Mater. Chem.* **2011**, *21*, 1822. Taj, S. F.; Singer, R.; Nazir, T.; Williams, G. R. *RSC Adv.* **2013**, *3*, 358.

(17) Chui, S. S.-Y.; Lo, S. M.-F.; Charmant, J. P. H.; Orpen, A. G.; Williams, I. D. *Science* **1999**, *283*, 1148.

(18) Gotthardt, M. A.; Schoch, R.; Wolf, S.; Bauer, M.; Kleist, W. *Dalton Trans.* **2015**, *44*, 2052.

(19) Peterson, G. W.; Wagner, G. W.; Balboa, A.; Mahle, J.; Sewell, T.; Karwacki, C. J. *J. Phys. Chem. C* **2009**, *113*, 13906. Wong-Foy, A. G.; Matzger, A. J.; Yaghi, O. M. *J. Am. Chem. Soc.* **2006**, *128*, 3494.

(20) Secco, E. A.; Worth, G. G. *Can. J. Chem.* **1987**, *65*, 2504.

(21) Morioka, H.; Tagaya, H.; Karasu, M.; Kadokawa, J.; Chiba, K. *Inorg. Chem.* **1999**, *38*, 4211.

(22) Parsons, G. N.; George, S. M.; Knez, M. *MRS Bull.* **2011**, *36*, 865.

(23) Zhao, J.; Losego, M. D.; Lemaire, P. C.; Williams, P. S.; Gong, B.; Atanasov, S. E.; Blevins, T. M.; Oldham, C. J.; Walls, H. J.; Shepherd, S. D.; Browe, M. A.; Peterson, G. W.; Parsons, G. N. *Adv. Mater. Interfaces* **2014**, *1*, 1400040. Zhao, J.; Gong, B.; Nunn, W. T.; Lemaire, P. C.; Stevens, E. C.; Sidi, F. I.; Williams, P. S.; Oldham, C. J.; Walls, H. J.; Shepherd, S. D.; Browe, M. A.; Peterson, G. W.; Losego, M. D.; Parsons, G. N. *J. Mater. Chem. A* **2015**, *3*, 1458.

DOI: 10.1021/jacs.5b08752
J. Am. Chem. Soc. 2015, 137, 13756–13759